PHYSICS AND CHEMISTRY OF SOLID STATE
V. 27, No. 2 (2026) pp. 409-419
Section: Physics

DOI: 10.15330/pcss.27.2.409-419

Vasyl Stefanyk Carpathian National University

ФІЗИКА І ХІМІЯ ТВЕРДОГО ТІЛА
Т. 27, № 2 (2026) С. 409-419
Фізико-математичні науки

PACS: 75.70.-i

ISSN 1729-4428 (Print)
ISSN 2309-8589 (Online)

Ihor Stolyarchuk[1], Oleh Kuzyk[1], Ireneusz Stefanuik[2], Olesya Dan'kiv[1], Andriy Popovych[1], Andriy Stolyarchuk[1]

Structural, optical and magnetic studies of the thin films and nanoparticles of ZnCoO prepared by pulsed laser ablation

[1]*Drohobych Ivan Franko State Pedagogical University, Drohobych, Ukrain, i.stolyarchuk@dspu.edu.ua*
[2]*University of Rzeszo, Rzeszow, Poland*

Pulsed laser ablation has been applied for fabrication of $Zn_{1-x}Co_xO$ thin films and nanostructures with a cobalt content of up to 10%. X-ray diffraction studies indicate that all samples are crystalised in a hexagonal wurtzite structure with a preferred orientation along the (002) plane. No other peaks corresponding to cobalt clusters or cobalt oxide were detected. Atomic forse microscopy (AFM) and scanning electron microscopy (SEM) was used for characterization of obtained samples. The energy bandgap decrease with an increase of Co dopant concentration, which is due to the exhibition of the s,p–d exchange interaction. In the long-wavelength region of the spectrum the additional absorption is observed, with are explained in terms of d–d transitions in tetrahedrally coordinated Co^{2+} ions. In photoluminescence spectra, four main peaks were revealed, which are ascribed to near band gap emission and nterstitial zinc, oxygen vacancies, and other impurities and defects, not only in the bulk but also on the surfaces of the investigated samples. Electron paramagnetic resonance studies have confirmed ferromagnetic ordering in $Zn_{1-x}Co_xO$ thin films and nanoparticles at room temperatures. One of the most probable mechanisms for the origin of ferromagnetic ordering is the bound magnetic polaron model.

Keywords: ZnCoO, diluted magnetic semiconductor, pulsed laser ablation in liquids, thin film, nanoparticle, optical absorption, photoluminescence, electron paramagnetic resonance.

Received 07 January 2026; Accepted 17 June 2026; Published 30 June 2026.

Introduction

Oxide-based diluted magnetic semiconductors (DMSs) have recently attracted significant attention due to their promising magnetic properties. A key challenge for the practical application of these materials is achieving ferromagnetism (FM) at temperatures above room temperature (RT). Zinc oxide (ZnO), a wide-bandgap semiconductor with a wurtzite structure (Eg ≈ 3.36 eV), doped with transition metals (TMs), has been theoretically proposed as a promising DMSs candidate for spintronic applications operating at room temperature [1–5].

Among the numerous oxide magnetic nanoparticle systems (MNPs), considerable attention is paid to zinc oxide MNPs doped with cobalt ions. Such interest is primarily due to the manifestation of ferromagnetic properties at temperatures close to room temperature and the prospects for the practical application of such structures [6,7].

An additional modification of the energy spectrum, as well as of the s,p–d, and d–d exchange interactions responsible for the unique magnetic and magneto-optical properties of oxide DMSs, can also be achieved by reducing the system's dimensionality [8,9].

The modern development of semiconductor materials science is characterized by a wide variety of technological methods for fabricating quantum-dimensional structures. In particular, it is worth noting the significant progress achieved over the past decades in the development of molecular beam techniques, which enable high structural quality, especially at interfaces [10–13]. However, such methods are complex and expensive, which limits their widespread application. In this regard, alternative approaches are technological methods based on laser

radiation, which are widely used for the growth of both thin semiconductor films and nanostructures [14–16].

Several terms have been proposed for laser-based techniques [17,18], such as “pulsed laser deposition”, “pulsed laser evaporation”, “laser ablation”, “laser epitaxy”, etc. It is worth noting several fundamental features that distinguish laser techniques from other technological methods: virtually any materials in different aggregate states can be evaporated under laser irradiation; the energy of atoms or ions formed in the plasma during the interaction of laser radiation with matter can range from several to hundreds of eV, which improves the conditions for laser epitaxy; the possibility of depositing quantum-sized structures in a “pulse-by-pulse” mode, which ensures precise control over the thickness of the grown layer; etc. Another important factor is the growth rate in laser deposition, estimated at about 0.5 Å per pulse.

In this work, we present the results of a study of the structural, optical, and magnetic properties of thin films and nanostructures of $Zn_{1-x}Co_xO$ prepared by pulsed laser ablation.

I. Materials and methods

The schematic diagram of the setup used for thin film deposition is shown in Fig. 1. The sources of laser radiation were an excimer XeCl laser (Lambda Physik LPX 315) and a solid-state Nd:YAG laser operating in a pulsed mode. Their main parameters are listed in Table 1.

Table 1.
Main characteristics of the lasers used for the obtained of thin films and nanostructures

Laser type	Excimer XeCl laser	Solid-state Nd:YAG laser
Radiation wavelength	λ = 308 nm	λ = 1060 nm
Laser radiation energy density	200 mJ/cm²	10 J/cm²
Pulse duration	30 ns	10 ns
Repetition rate	10 Hz	10 Hz

To increase the radiation flux density, the laser beam was further focused onto the target surface using a lens system. The laser beam was incident on the target surface at 45°. To ensure uniform conditions of material evaporation under laser irradiation, the target was driven by a stepper motor (inset in Fig. 1a). The chamber was evacuated to a residual pressure of 10^{-7} Torr using a turbomolecular pump.

The growth chamber was also equipped with a substrate heater (20–350 °C) and a quadrupole mass spectrometer. The material evaporated under high-power laser radiation was deposited onto the substrates. The distance between the substrate and the target was optimized during the experiments and ranged from 15 mm to 30 mm. Borosilicate glass, crystalline sapphire, and quartz were used as substrate materials. To determine the optimal deposition regimes and expand the range of studied samples, a series of experiments was conducted with varying numbers of laser pulses (50-5000).

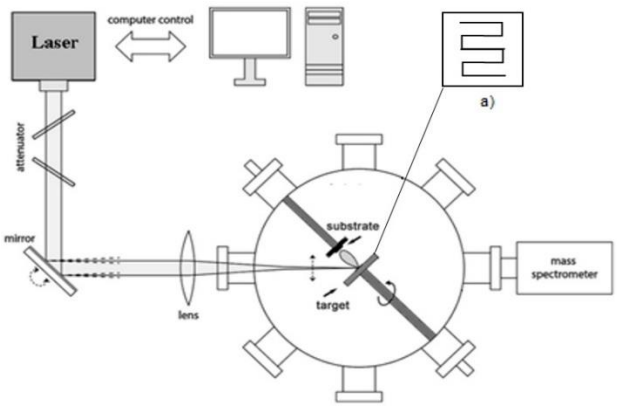

Fig. 1. Schematic diagram of the setup for the growth of semiconductor thin films: 1 – target, 2 – substrate, 3 – lens system for focusing the laser radiation, 4 – laser. The inset (a) shows the trajectory of the laser beam on the target surface.

Solid solutions of substitution Zn–Co–O of various compositions, obtained by solid-state mixing of the corresponding oxides or carbonates, were used as targets. ZnO and $CoCO_3$ (analytical grade) were used as starting materials without additional purification. The initial components were loaded into a ball mill, followed by mechanosynthesis in ethanol and drying at 100 °C for 1 h, and subsequent annealing in air at 700 °C for 4 h. To homogenize the obtained targets, an additional ball-milling step in ethanol was performed, followed by drying in air at 100 °C for 1 h.

As a result, a grain size in the range of 20–50 nm was obtained. Under the influence of electrostatic forces, the resulting powder mixture agglomerates into clusters with an average size of 0.4–0.8 μm. This stoichiometric mixture was loaded into graphite molds measuring 15–40 mm under 100 MPa of pressure. The pellets were sintered in a muffle furnace in air. After sintering, the samples were cooled to room temperature for 10–15 h. It was experimentally established that rapid cooling within 10–15 min leads to deterioration of the mechanical properties of the targets.

The pulsed laser ablation in liquid (PLAL) method is used for the synthesis of metallic nanoparticles [19] and binary semiconductor particles [20,21]. We have proposed, for the first time, the use of the PLAL method for the synthesis of nanoparticles of diluted magnetic semiconductors. Using this method, nanostructures of $Cd_{1-x}Mn_xTe$ and ZnO:Me (Me: Mn, Co) were obtained [15, 22].

The schematic diagram of the PLAL setup is shown in Fig. 2. As in pulsed laser deposition, XeCl and Nd:YAG lasers operating in pulsed mode were used.

To ensure uniform thermodynamic conditions for nanoparticle synthesis, particularly in the laser-plasma-liquid environment, a rotating mirror was mounted on a specially designed holder. This holder consisted of a stage and stepper motors that rotated the stage (and the mirror mounted on it) in both vertical and horizontal directions. This ensured that each laser pulse interacted directly with the target surface over a 7 × 7 mm area.

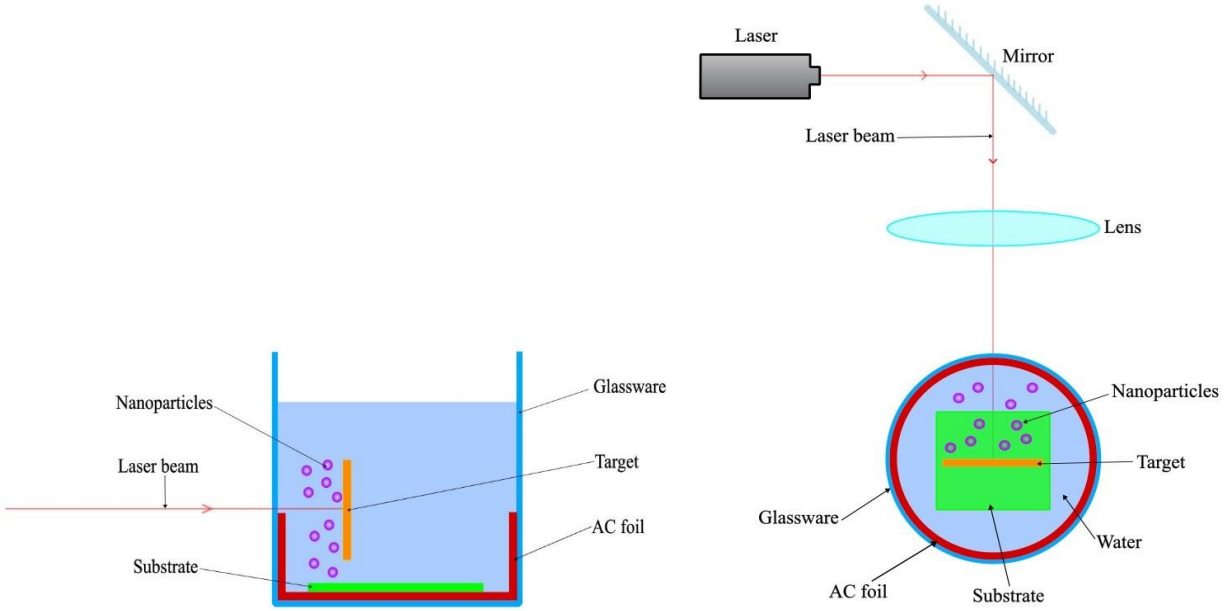

Fig. 2. Schematic diagram (in two planes) of the setup for the synthesis of $Zn_{1-x}Co_xO$ nanoparticles by pulsed laser ablation in liquid.

II. Results and discussion

First, the grown of the thin films and synthesized nanoparticles of $Zn_{1-x}Co_xO$ were subjected to structural analysis to verify the absence of secondary phases. Figure 3 shows the X-ray diffraction pattern of $Zn_{1-x}Co_xO$ thin films and nanoparticles deposited on a glass substrate. The studies were carried out using a D8 ADVANCE X-ray Diffractometer with DAVINCI, employing Cu–Kα radiation (λ = 1.54059 Å) and scanning over the 2θ range from 10° to 70°.

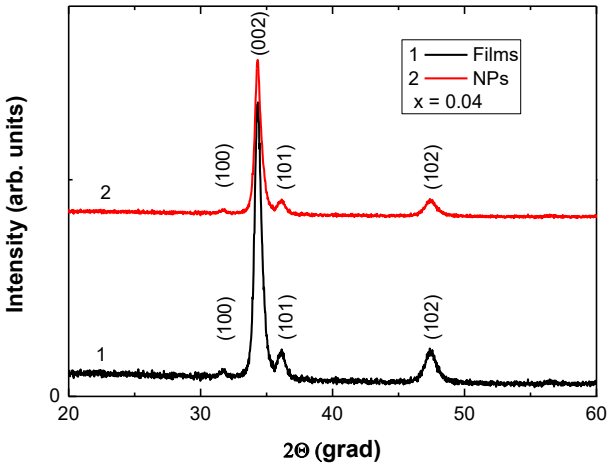

Fig. 3. XRD spectra of $Zn_{1-x}Co_xO$ thin films and nanoparticles.

The results indicate that the synthesized films and nanoparticles possess a hexagonal wurtzite-type ZnO structure, with a preferred (002) orientation and the hexagonal c-axis as the preferred orientation. With increasing concentration of the magnetic dopant, additional peaks corresponding to the (100), (101), and (102) orientations of the initial ZnO were observed. At the same time, an increase in the diffraction peak intensity was observed, indicating an improvement in the crystalline structure of the studied samples. No other peaks corresponding to cobalt clusters or cobalt oxide were detected, which indicates the substitution of Zn^{2+} ions by Co^{2+} ions in the crystal lattice. For all investigated samples, a slight shift in the angular position of the (002) reflection was also observed, whereas the positions of the other reflections remained unchanged with increasing dopant concentration. For concentrations $x \leq 4\%$, the peak shifted toward lower 2θ values, indicating that the obtained quantum-sized structures are under uniform strain. With further increase in cobalt concentration, the (002) peak shifted in the opposite direction, indicating a change in the nature of the strain. The obtained results, as well as the close values of the ionic radii in tetrahedral coordination (for example, 0.058 nm for Co^{2+} ions and 0.06 nm for Zn^{2+} ions), provide additional confirmation of the substitution of Zn^{2+} ions by 3d Co^{2+} ions in the crystal lattice without a change in its crystal structure.

Morphological studies of the surface of the films, as well as of the nanoparticles deposited on aluminum foil, carried out using atomic force microscopy (AFM), are presented in Fig. 4. In our studies, atomic force microscopes manufactured by Anfatec, NT-MDT, and Nanotec Electronica S.L. were used. In the majority of experiments, the semi-contact mode was employed.

Cantilevers with a resonance frequency of about 150 kHz, a tip curvature radius of 10 nm, and an apex angle of ≤ 22° were used. On the surface of $Zn_{1-x}Co_xO$ films (Fig. 4a), islands with heights up to 140 nm and a root-mean-square roughness of R_{ms} = 55 nm are observed. Increasing the substrate temperature from 270 °C to 300°C reduces the height of the surface features to 80 nm and the R_{ms} to 30 nm. At the same time, an increase in the partial pressure of oxygen leads to an increase in the root-mean-square surface roughness. An increase in cobalt concentration does not lead to a significant change in their sizes.

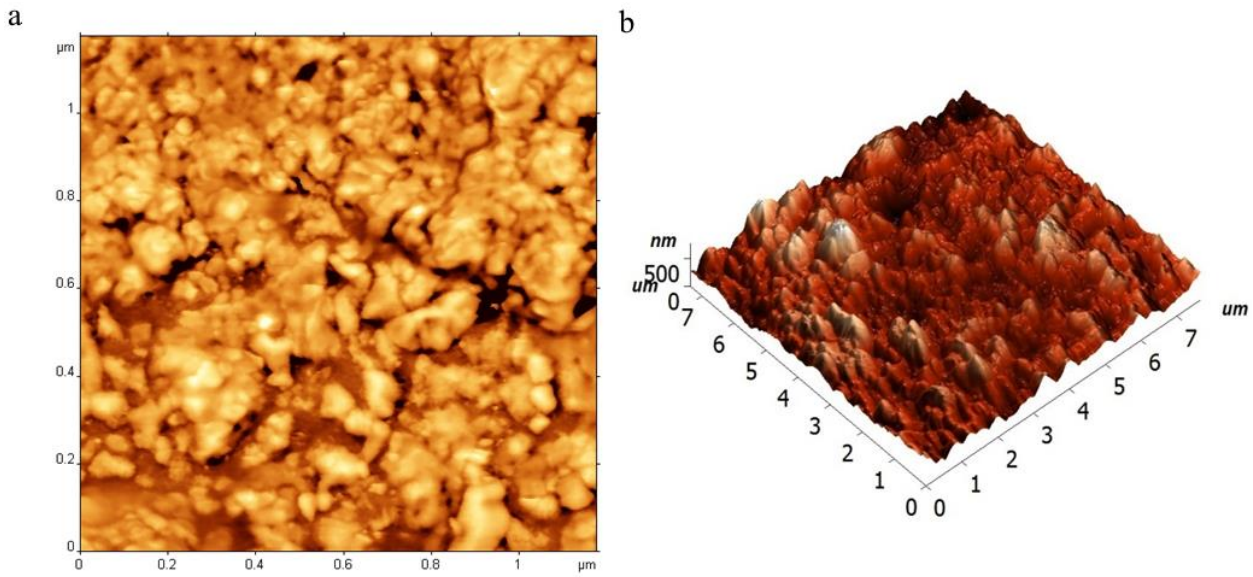

Fig. 4. AFM images of $Zn_{1-x}Co_xO$: (a) 2D image of thin films, (b) 3D image of nanoparticles.

The AFM images of $Zn_{0.98}Co_{0.02}O$ nanostructures shown in Fig. 4b demonstrate a variation in the size distribution of the nanoparticles without providing detailed information about their shape and structure. The particle sizes estimated from these AFM images range from 20 to 80 nm.

Scanning electron microscopy (SEM) studies of colloidal suspensions containing $Zn_{1-x}Co_xO$ nanoparticles indicate the formation of a complex structure in which, in addition to isolated nanoparticles, agglomerated formations are also present, whose shape resembles flowers (Fig. 5). These flower-like formations, in turn, consist of nanosheets with a thickness of 5–10 nm and a diameter of 20–50 nm. Similar results, namely the formation of flower-like nanostructures, were obtained during the synthesis of ZnMnO nanoparticles [15] and zinc oxide nanostructures by chemical methods [23–25].

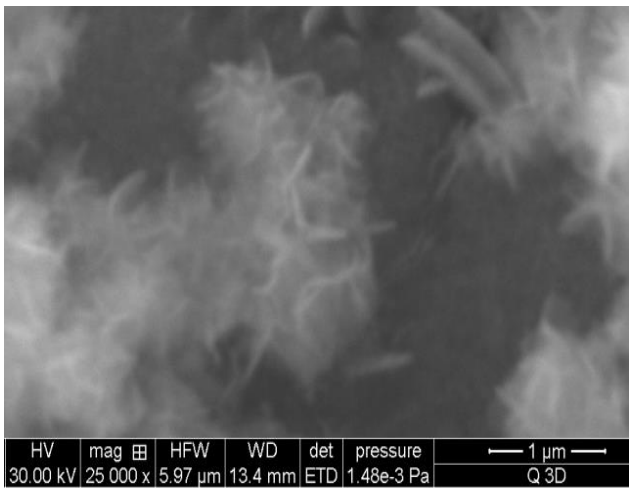

Fig. 5. SEM image of a colloidal suspension containing $Zn_{1-x}Co_xO$ nanocrystals obtained by laser ablation in deionized water

The optical properties of $Zn_{1-x}Co_xO$ thin films were studied on glass, quartz, and sapphire substrates. The corresponding spectra were recorded without separating the film from the substrate; therefore, a correction for the substrate contribution was applied in the calculations. Figure 6 shows the transmission spectra of $Zn_{1-x}Co_xO$ thin films deposited on a glass substrate. A characteristic feature of these spectra is the appearance of the intrinsic absorption edge only in samples with low x values ≤ 0.04.

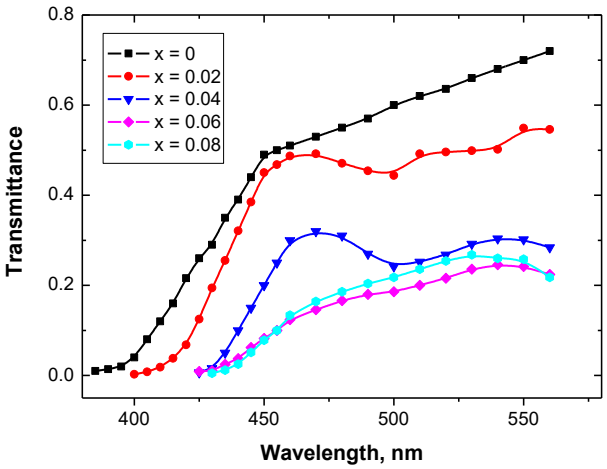

Fig. 6. Transmission spectrum of $Zn_{1-x}Co_xO$ thin films deposited on a glass substrate by the ion–plasma method.

With the incorporation of cobalt ions into the ZnO lattice and an increase in their concentration, the fundamental absorption edge shifts toward the long-wavelength region of the spectrum. A similar behavior of the band gap width has been observed for $Zn_{1-x}Co_xO$ films obtained by various methods [26–28]. This band-gap behavior is due to the influence of the s,p–d exchange interaction, which leads to negative and positive shifts of the conduction and valence band edges, respectively, resulting in a corresponding decrease in the band gap width [29].

At the same time, as the cobalt concentration increases, an additional absorption mechanism becomes increasingly significant, spanning the wavelength range from 500 to 750 nm. For samples with cobalt content up to 6%, a fine structure of additional absorption is observed in the long-wavelength region of the spectrum, with bands at 568, 616, and 660 nm. These three absorption peaks are

explained in terms of d–d transitions in tetrahedrally coordinated Co^{2+} ions. In particular, the absorption peaks are attributed to the following transitions: $^4A_3(F) \rightarrow {}^2E(G)$, $^4A_3(F) \rightarrow {}^4T_1(P)$, and $^4A_2(F) \rightarrow {}^2A_1(G)$.

A similar behavior of the absorption edge with increasing cobalt concentration is also observed for $Zn_{1-x}Co_xO$ nanoparticles (Fig. 7). In addition to the short-wavelength shift of the spectrum caused by the quantum size effect, a decrease in the band gap width with increasing content of Co^{2+} ions is observed, which is due to the manifestation of the s,p–d exchange interaction. As in the case of thin films, a fine structure in the absorption spectrum in the long-wavelength region is observed for $Zn_{1-x}Co_xO$ nanocrystals with $x \leq 0.06$, with absorption bands at wavelengths of 565 nm and 654 nm (Fig. 8). This structure is associated with d–d transitions of Co^{2+} ions located in a tetragonal crystal field and corresponds to the transitions: $^4A_1(F) \rightarrow {}^2A_1(G)$ and $^4A_2(F) \rightarrow {}^2E(G)$.

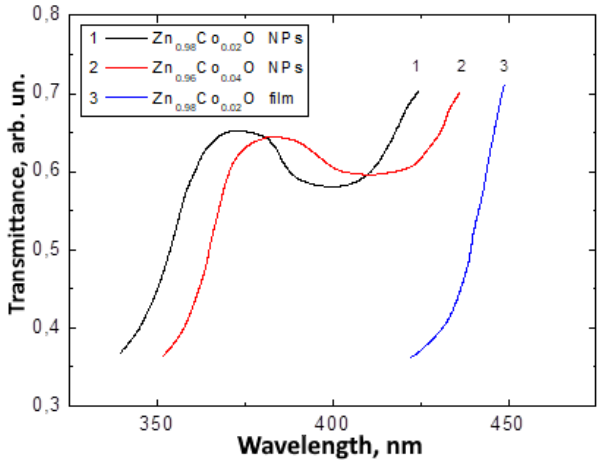

Fig.7. Transmission spectra of $Zn_{1-x}Co_xO$ nanocrystals obtained by pulsed laser ablation in liquid:
1 – x = 0.02, 2 – x = 0.04, 3 – thin film with x = 0.02.

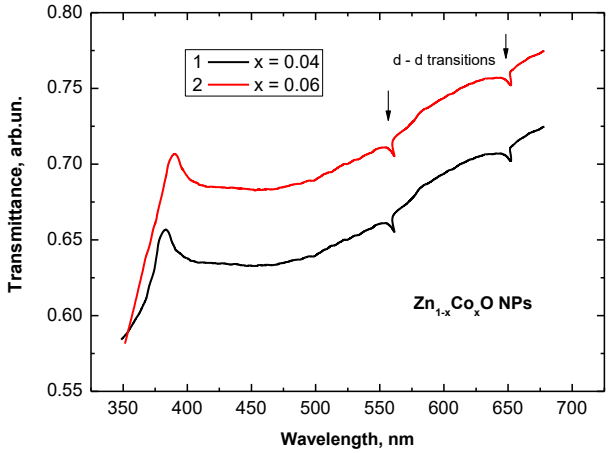

Fig. 8. Transmission spectrum of $Zn_{1-x}Co_xO$ nanocrystals in the long-wavelength region corresponding to d–d transitions.

Using the effective mass approximation, we analyzed the absorption spectrum of $Zn_{1-x}Co_xO$ nanocrystals. The determined energy shift is in good agreement with the analytical approximation obtained in [30,31] for the 1s excitonic states of nanocrystals with an average radius:

$$E_{1s} = E_g^{bulk} + \frac{\pi^2 h^2}{2er^2}\left(\frac{1}{m_e^*} + \frac{1}{m_h^*}\right) - \frac{1.8e^2}{4\pi\varepsilon\varepsilon_0 r} \qquad (1)$$

where r is the radius of the nanoparticles, E_g^{bulk} is the band gap of the bulk crystal, m_e^* and m_h^* are the effective masses of the electron and hole, respectively, e is the electron charge, ε is the relative dielectric permittivity, and ε_0 is the vacuum permittivity.

Using the values $m_e = 0.21$, $m_h = 0.8$ and $\varepsilon = 8.3$ as for bulk ZnO, and by substituting the experimentally determined energy shift $\Delta E = 0.64$ eV, the average radius of the nanoparticles (1) is estimated as R = 18 nm. These values are in good agreement with the data obtained from SEM studies.

Photoluminescence spectroscopy is a sensitive, non-destructive method for studying the optical properties of semiconductors and investigating both intrinsic and extrinsic defects. It provides information about the energy states of impurities and defects even at very low concentrations, which is extremely important for understanding the influence of structural defects on the properties of semiconductor nanostructures.

The optical properties during the transition from bulk crystals to quasi-two-dimensional structures are largely determined by the fabrication conditions (temperature, substrate type, annealing temperatures, pressure, etc.). These same factors also affect the photoluminescence spectra of quantum-sized structures, especially in the visible region. This is because, in this region, the emission bands are governed by defects and impurities present both in the bulk and on the surface.

The photoluminescence excitation was performed using a He-Cd laser with a wavelength of $\lambda = 325$ nm and a nominal power of 10 mW.

Figure 9 shows the photoluminescence spectra of $Zn_{1-x}Co_xO$ thin films deposited on glass and quartz substrates. At room temperature, all samples exhibit four emission bands in the 2.0–3.4 eV energy range. The first band in the ultraviolet region of the spectrum (at $\lambda = 386$ nm) is due to excitonic transitions near the fundamental absorption edge [32]. With increasing cobalt concentration, the maximum of this band undergoes a red shift, which is caused by the exchange interaction between the d-electrons of impurity ions and the s- and p-carriers of the corresponding bands and is in good agreement with the results of transmission-spectroscopy studies.

The emission band with a maximum at 426 nm is most likely associated with transitions between radiative defect states and the valence band [33]. An unambiguous interpretation of the emission band in the blue region ($\lambda = 443$ nm) of the spectrum is rather difficult. The authors of [34] observed such a band for ZnO nanodisks obtained by the hydrothermal method and attribute it to electronic transitions from ionized oxygen vacancy levels to the valence band. At the same time, this wavelength range also includes an emission band associated with surface defects in zinc oxide [35]. The authors of [36] and [37] identify this band with transitions between interstitial zinc (Zn_i) and the valence band. Another group of authors [38] associates this blue emission band with transitions from interstitial cobalt levels to the valence band.

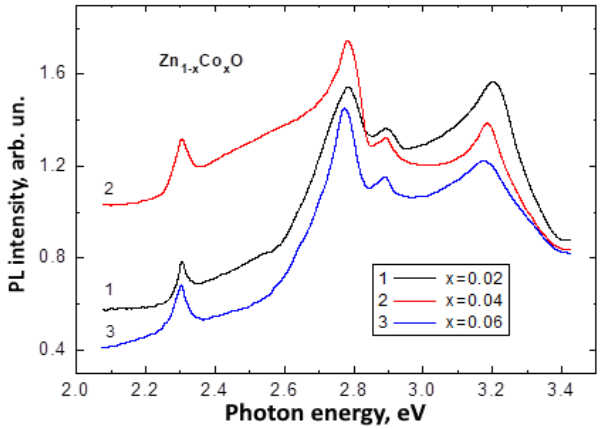

Fig. 9. Photoluminescence spectra of $Zn_{1-x}Co_xO$ thin films at room temperature:
1 – x = 0.02; 2 – x = 0.04; 3 – x = 0.06.

It should be noted that a slight red shift of this band (from 443 nm to 448 nm) with increasing Co content may support this interpretation. The emission band with a maximum at 538 nm can be unambiguously attributed to transitions from ionized oxygen vacancies (V_O) to the valence band [39].

A similar behavior is also observed in the photoluminescence spectra of $Zn_{1-x}Co_xO$ nanoparticles (Fig. 10). Four emission bands with maxima at wavelengths of 390 nm, 414 nm, 503 nm, and 540 nm are distinguished in the spectra. The shortest-wavelength emission band in the spectrum is due to excitonic transitions at the fundamental absorption edge. With increasing cobalt content, this band undergoes a slight red shift, in good agreement with results from optical absorption spectra.

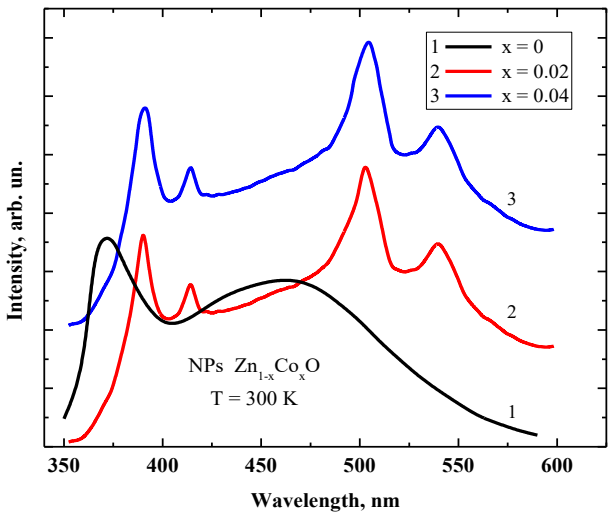

Fig. 10. Photoluminescence spectra of $Zn_{1-x}Co_xO$ nanocrystals obtained by PLAL at T = 300 K:
1 – x = 0; 2 – x = 0.02, 3 – x = 0.04.

The other bands observed in the photoluminescence spectra are associated with impurities and defects within the nanoparticles. The emission band in the violet–blue region of the spectrum (centered at 414 nm) can be interpreted as transitions from radiative defect states associated with interstitial zinc (Zn_i) or zinc vacancies (V_{Zn}) formed at the surface to the valence band [33].

As in the case of thin films, the interpretation of the emission band in the blue region of the spectrum is the most complex. As mentioned above, the authors of [36] attribute this band to transitions between interstitial zinc (Zn_i) levels and the valence band. Studies of ZnO nanoparticles obtained by the hydrothermal method [34] demonstrate an emission band in this wavelength range and associate it with electronic transitions from ionized oxygen vacancy levels to the valence band. At the same time, this wavelength range also includes an emission band related to transitions from interstitial cobalt levels to the valence band, as reported in [38].

An additional argument in favor of this interpretation is a slight shift of the band maximum (from 502 nm to 506 nm) with increasing cobalt concentration. The emission band with a maximum at 540 nm can, as in the case of thin films, be unambiguously attributed to the presence of oxygen vacancies, i.e., transitions from ionized oxygen vacancies (V_O) to the valence band [39].

It should also be noted that another feature observed in all the investigated photoluminescence spectra of nanostructures. The emission bands corresponding to the visible wavelength range are asymmetric. This behavior is due to defect states at the surface and in the bulk of the investigated diluted magnetic oxide semiconductor $Zn_{1-x}Co_xO$ nanoparticles.

One of the most convenient and highly sensitive methods for obtaining information on the charge state, spatial distribution, and interactions of magnetic impurities with the semiconductor matrix is electron paramagnetic resonance (EPR).

Electron paramagnetic resonance spectra in the X-band were recorded on a Bruker Elexsys 580 FT/CW spectrometer (9.3 GHz, 100 kHz magnetic field modulation, 0.05 mT modulation amplitude). Temperature-dependent EPR measurements were performed over 100–350 K using a Bruker ER4131VT cryogenic system with Bruker Elexsys software.

Figure 11 shows the temperature dependence of the electron paramagnetic resonance spectra of $Zn_{0.96}Co_{0.04}O$ thin films. For all investigated $Zn_{1-x}Co_xO$ films with a concentration $x \leq 0.1$, the EPR spectra are characterized by a broad asymmetric line of Dyson shape and are satisfactorily described by a Lorentzian-type curve with a Dyson term [40, 41]. A decrease in temperature reduces the intensity of the resonance line and increases its linewidth. Such behavior is characteristic of ferromagnetic materials [42]. At temperatures close to ferromagnetic ordering, a transformation of the spectra is observed, caused by a further splitting of the broad asymmetric band into two Dyson lines.

Direct information about the magnetic states can be obtained from the temperature dependence of the integral intensity of the electron paramagnetic resonance spectrum. The integral intensity is proportional to the spin susceptibility of the paramagnetic centers participating in the resonance.

Figure 12 shows the temperature dependence of the inverse integral intensity of the ferromagnetic resonance signal in a $Zn_{0.98}Co_{0.02}O$ film. The intensity was determined from the first derivative of the absorption line transformed to a Lorentzian type [43,44].

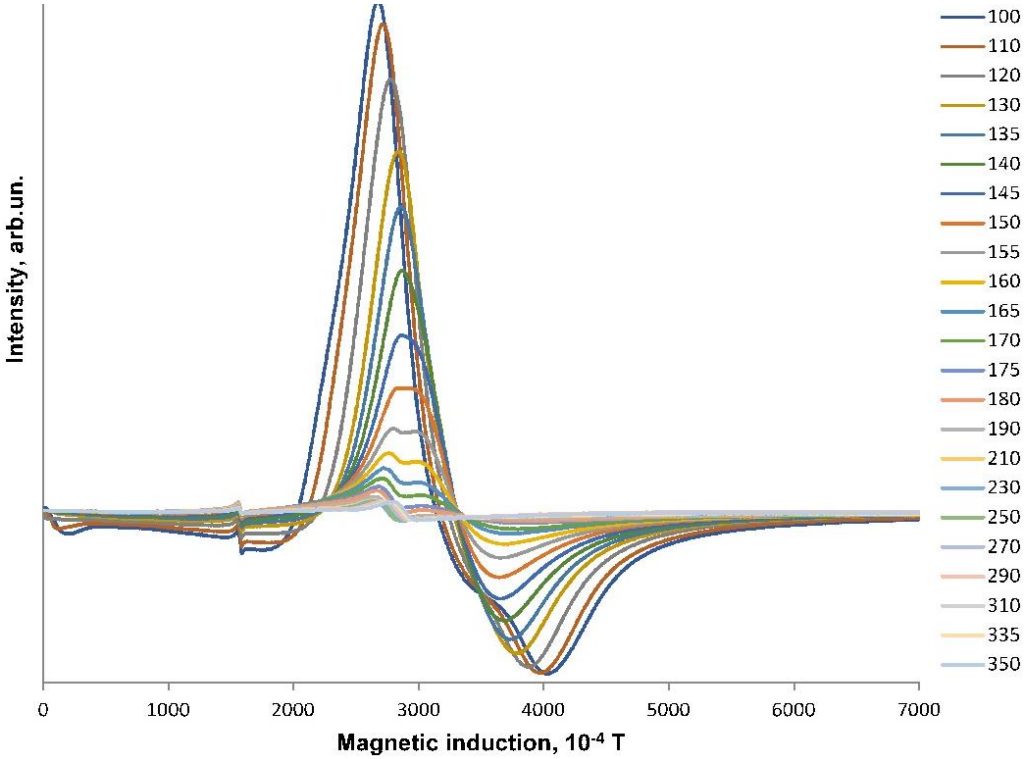

Fig. 11. Temperature dependence of the electron paramagnetic resonance spectra of $Zn_{0.96}Co_{0.04}O$ thin films.

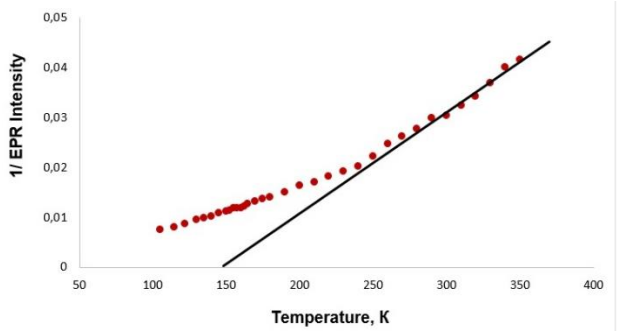

Fig. 12. Temperature dependence of the inverse EPR signal intensity for $Zn_{0.96}Co_{0.04}O$ thin films.

For the analysis of the temperature dependence of the integral intensity, which is proportional to the magnetic susceptibility, we used the Curie–Weiss law. The linear increase of with temperature is consistent with the Curie–Weiss law:

$$(\chi - \chi_0)^{-1}(T) = (T-\theta_{CW})/C \qquad (2)$$

where C is the Curie constant, which depends on the type of material, θ_{CW} is the paramagnetic Curie temperature, and χ_0 is the temperature-independent magnetic susceptibility of the diamagnetic matrix and other Pauli-type paramagnetic contributions.

Linear extrapolation of the high-temperature region of the inverse integral intensity enabled the determination of the Curie–Weiss temperature for the investigated samples. It amounts to T_c = 148.6 K for $Zn_{0.96}Co_{0.04}O$ films. The positive Curie–Weiss temperature unambiguously indicates ferromagnetic ordering in the studied films.

The magnetic properties were also investigated using the electron paramagnetic resonance method for $Zn_{1-x}Co_xO$ nanoparticles ($x \leq 0.06$) obtained by pulsed laser ablation in liquid. Figure 13 shows the temperature dependences of the EPR spectra for $Zn_{0.98}Co_{0.02}O$ nanoparticles. As in the case of $Zn_{1-x}Co_xO$ thin films, a decrease in temperature leads to a broadening of the line and an increase in its asymmetry. At the same time, the shape of the resonance line is more satisfactorily described by a Lorentzian profile. Such behavior of the resonance line indicates ferromagnetic ordering in the studied nanostructures.

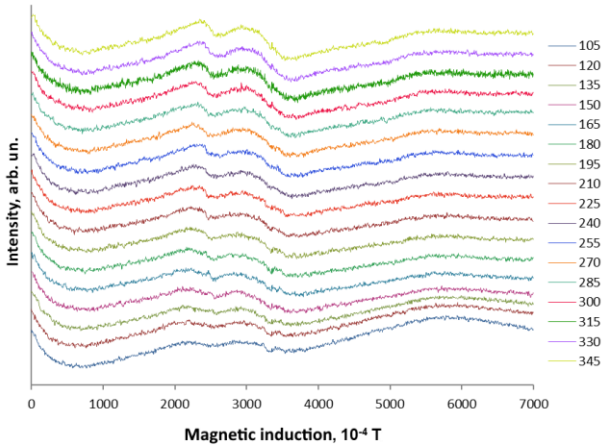

Fig. 13. Temperature dependence of the electron paramagnetic resonance spectra of $Zn_{0.98}Co_{0.02}O$ nanoparticles.

Table 2 presents the temperature dependences of the ferromagnetic resonance parameters of $Zn_{0.98}Co_{0.02}O$ nanoparticles: the linewidth , the resonance field , and the signal amplitude. The amplitude depends linearly on

temperature, whereas the temperature behavior of and is more complex. In general, both ferromagnetic resonance characteristics demonstrate temperature dependences typical for nanoparticles with magnetic ordering [45].

Table 2.

Parameters of the EPR spectra of $Zn_{0.98}Co_{0.02}O$ nanoparticles

T (K)	B_{pp} (mT)	B_{res} (mT)	A	g
300	64.94	322.13	5.578	2.084456
290	73.5	319.55	5.533	2.101286
270	76.53	325.535	5.47555	2.062654
250	74.9	322.25	5.314	2.08368
230	78.69	320.045	4.97485	2.098036
210	80.31	317.845	4.71485	2.112558
190	76.2	320.2	4.26225	2.09702
170	68.38	316.99	4.0065	2.118256
150	61.52	320.42	3.6601	2.095581
130	32.72	313.54	3.013	2.141564
110	91.963	316.4815	3.0171	2.121659
90	59.11	299.045	2.3198	2.245368
80	34.85	311.875	2.02085	2.152997
70	55	301.1	1.7925	2.230043

The mechanism responsible for the observed ferromagnetism in the studied quantum-sized structures has not yet been clearly established, and its origin remains a matter of debate. At present, several theories exist regarding the manifestation of ferromagnetic ordering in wide-bandgap diluted magnetic semiconductors. One of the recently proposed models for explaining the emergence of ferromagnetic ordering in oxide DMSs is the bound magnetic polaron model [46,47].

The magnetic (ferromagnetic) behavior observed in $Zn_{1-x}Co_xO$ quantum-sized structures is interpreted within the framework of the aforementioned bound magnetic polaron model. An additional argument in favor of this model is provided by the presence of oxygen vacancies in the studied thin films and nanostructures, as revealed by photoluminescence and EPR studies.

Conclusions

Structural studies of $Zn_{1-x}Co_xO$ thin films and nanocrystals carried out using X-ray diffraction indicate the formation of quantum-sized structures of oxide diluted magnetic semiconductors with a wurtzite structure and a preferred orientation along the (002) direction of the hexagonal c-axis.

The formation of a complex structure of $Zn_{1-x}Co_xO$ nanoparticles obtained by pulsed laser ablation in liquid has been established, in which, in addition to isolated nanoparticles, agglomerated formations are also present, whose shape resembles flowers and which consist of nanosheets with a thickness of 5–10 nm and a diameter of 20–50 nm.

Optical spectroscopy methods have revealed features in the absorption spectra of $Zn_{1-x}Co_xO$ films and nanoparticles at the fundamental absorption edge, arising from the s,p–d exchange interaction. In the long-wavelength region of absorption of $Zn_{1-x}Co_xO$ thin films and nanocrystals, a fine absorption structure has been observed, which is identified within the framework of the model of intracenter d–d transitions of 3d Co^{2+} ions.

Photoluminescence spectroscopy studies of thin films and nanoparticles have enabled the identification of interstitial zinc, oxygen vacancies, and other impurities and defects, not only in the bulk but also on the surfaces of the investigated samples.

Electron paramagnetic resonance studies have confirmed ferromagnetic ordering in $Zn_{1-x}Co_xO$ thin films and allowed determination of the Curie temperature, which is T_c=148.6 K. A ferromagnetic behavior has also been established for $Zn_{1-x}Co_xO$ nanoparticles ($x \leq 0.06$) obtained by pulsed laser ablation in liquid. One of the most probable mechanisms for the origin of ferromagnetic ordering is the bound magnetic polaron model.

Stolyarchuk Ihor – Doctor of Physical and Mathematical Sciences, Professor;
Kuzyk Oleg – Candidate of Physical and Mathematical Sciences, Associate Professor;
Stefanuik Ireneusz – Dr., Prof.;
Dan'kiv Olesya – Candidate of Physical and Mathematical Sciences, Associate Professor;
Popovych Andriy – Lecturer, Department of Physics and Information Systems;
Stolyarchuk Andriy – PhD student.

[1] T. Dietl, H. Ohno, F. Matsukura, J. Cibert, and D. Ferrand, *Zener Model Description of ferromagnetism in Zinc-Blende magnetic semiconductors*, Science 287, 1019 (2000); https://doi.org/10.1126/science.287.5455.1019.
[2] Q. Wang, Q. Sun, P. Jena, and Y. Kawazoe, *Carrier-mediated ferromagnetism in N codoped (Zn,Mn)O(*$10\bar{1}0$*)thin films*, Physical Review B, 70, (2004); https://doi.org/10.1103/PhysRevB.70.052408.
[3] S. W. Jung, S. -j. An, G.-C. Yi, C. U. Jung, S.-I. Lee, and S. Cho, *Ferromagnetic properties of* $Zn_{1-x}Mn_x$ *O epitaxial thin films*, Applied Physics Letters, 80, 4561 (2002); https://doi.org/10.1063/1.1487927.
[4] D. Anbuselvan, S. Nilavazhagan, A. Santhanam, N. Chidhambaram, K. V. Gunavathy, T. Ahamad, and S. M. Alshehri, Room temperature ferromagnetic behavior of nickel-doped zinc oxide dilute magnetic semiconductor for spintronics applications, Physica E Low-Dimensional Systems and Nanostructures, 129, 114665 (2021); https://doi.org/10.1016/j.physe.2021.114665.
[5] Y. Belghazi, M. A. Aouaj, M. E. Yadari, G. Schmerber, C. Ulhaq-Bouillet, C. Leuvrey, S. Colis, M. Abd-Lefdil, A. Berrada, and A. Dinia, *Elaboration and characterization of Co-doped ZnO thin films deposited by spray pyrolysis technique*, Microelectronics Journal, 40, 265 (2008); https://doi.org/10.1016/j.mejo.2008.07.051.

[6] S. Lardjane, G. Merad, N. Fenineche, A. Billard, and H. I. Faraoun, *Ab initio study of ZnCoO diluted magnetic semiconductor and its magnetic properties*, Journal of Alloys and Compounds, 551, 306 (2012); https://doi.org/10.1016/j.jallcom.2012.09.120.
[7] R. Hanafin and S. Sanvito, *Oxygen defect origin of ferromagnetism in ZnCoO*, Journal of Magnetism and Magnetic Materials, 322, 1209 (2009); https://doi.org/10.1016/j.jmmm.2009.05.030.
[8] D. Akcan, *Effect of type and concentration of cobalt precursor on structural, optical and defect properties of ZnCoO nanoparticles*, Materials Research Bulletin, 139, 111254 (2021); https://doi.org/10.1016/j.materresbull.2021.111254.
[9] G. Murtaza, Y. Abbas, and F. Ahmed, *Theoretical and experimental study of structural, electronic and optical properties of cobalt-doped zinc oxide*, Physica B Condensed Matter, 712, 417283 (2025); https://doi.org/10.1016/j.physb.2025.417283.
[10] B. P. Pamplin, Molecular Beam Epitaxy (1980); https://doi.org/10.1016/C2013-0-03272-0.
[11] A. C. Jones and P. O'Brien, Atomic Layer Epitaxy (1997). https://doi.org/10.1002/9783527614639.ch6.
[12] M. P. Soriaga, J. Stickney, L. A. Bottomley, and Y.-G. Kim, *Thin Films: Preparation, Characterization, Applications* (2002). https://doi.org/10.1007/978-1-4615-0775-8.
[13] R. K. Singh and J. Narayan, *Pulsed-laser evaporation technique for deposition of thin films: Physics and theoretical model,* Physical Review. B, Condensed Matter, 41, 8843 (1990); https://doi.org/10.1103/PhysRevB.41.8843.
[14] J. H. Kim, H. Kim, D. Kim, Y. E. Ihm, and W. K. Choo, *Magnetic properties of epitaxially grown semiconducting $Zn_{1-x}Co_xO$ thin films by pulsed laser deposition,* Journal of Applied Physics, 92, 6066 (2002); https://doi.org/10.1063/1.1513890.
[15] A. I. Savchuk, A. Perrone, A. Lorusso, I. D. Stolyarchuk, O. A. Savchuk, and O. A. Shporta, *ZnMnO diluted magnetic semiconductor nanoparticles: Synthesis by laser ablation in liquids, optical and magneto-optical properties*, Applied Surface Science, 302, 205 (2013); https://doi.org/10.1016/j.apsusc.2013.09.177.
[16] *Pulsed Laser Deposition of Thin Films* (2006). https://doi.org/10.1002/0470052120.
[17] Z. Yan and D. B. Chrisey, *Pulsed laser ablation in liquid for micro-/nanostructure generation*, Journal of Photochemistry and Photobiology C Photochemistry Reviews, 13, 204 (2012); https://doi.org/10.1016/j.jphotochemrev.2012.04.004.
[18] A. V. Simakin, V. V. Voronov, N. A. Kirichenko, and G. A. Shafeev, *Nanoparticles produced by laser ablation of solids in liquid environment*, Applied Physics A, 79, 1127 (2004); https://doi.org/10.1007/s00339-004-2660-8.
[19] R. Sabry, M. Fikry, O. S. Ahmed, A. R. N. Zekri, and A. F. Zedan, *Laser-Induced synthesis of pure zinc oxide nanoflakes*, Journal of Physics Conference Series, 1472, 012005 (2020); https://doi.org/10.1088/1742-6596/1472/1/012005.
[20] M. S. Shakeri et al., *Pulsed laser engineering of composite submicron particles in colloidal systems: A high-performance catalyst for ethanol fuel cells*, Composites Part B Engineering, 299, 112457 (2025); https://doi.org/10.1016/j.compositesb.2025.112457.
[21] P. K. Samanta, S. K. Patra, and P. R. Chaudhuri, *Violet emission from flower-like bundle of ZnO nanosheets*, Physica E Low-Dimensional Systems and Nanostructures, 41, 664 (2008); https://doi.org/10.1016/j.physe.2008.11.015.
[22] Ol. A. Savchuk, A. I. Savchuk, I. D. Stolyarchuk, P. M. Tkachuk, and V. I. Garasym, *Generation of diluted magnetic semiconductor nanostructures by pulsed laser ablation in liquid*, Proceedings of SPIE, the International Society for Optical Engineering/Proceedings of SPIE, 9809, 98090Y (2015); https://doi.org/10.1117/12.2228919.
[23] S. Chakraborty, A. K. Kole, and P. Kumbhakar, *Room temperature chemical synthesis of flower-like ZnO nanostructures*, Materials Letters, 67, 362 (2011); https://doi.org/10.1016/j.matlet.2011.10.018.
[24] P. Ramasamy and J. Kim, *Facile and fast synthesis of flower-like ZnO nanostructures*, Materials Letters, 93, 52 (2012); https://doi.org/10.1016/j.matlet.2012.11.042.
[25] J. H. Kim, H. Kim, D. Kim, S. G. Yoon, and W. K. Choo, *Optical and magnetic properties of laser-deposited Co-doped ZnO thin films*, Solid State Communications, 131, 677 (2004); https://doi.org/10.1016/j.ssc.2004.06.033.
[26] K. T. R. Reddy, V. Supriya, Y. Murata, and M. Sugiyama, *Effect of Co-doping on the properties of $Zn_{1-x}Co_xO$ films deposited by spray pyrolysis*, Surface and Coatings Technology, 231, 149 (2012); https://doi.org/10.1016/j.surfcoat.2012.05.064.
[27] S. Colis, H. Bieber, S. Bégin-Colin, G. Schmerber, C. Leuvrey, and A. Dinia, *Magnetic properties of Co-doped ZnO diluted magnetic semiconductors prepared by low-temperature mechanosynthesis*, Chemical Physics Letters, 422, 529 (2006); https://doi.org/10.1016/j.cplett.2006.02.109.
[28] J. A. Gaj and J. Kossut, *Introduction to the Physics of Diluted Magnetic Semiconductors* (2010). https://doi.org/10.1007/978-3-642-15856-8.
[29] A. D. Yoffe, *Low-dimensional systems: Quantum size effects and electronic properties of semiconductor microcrystallites (zero-dimensional systems) and some quasi-two-dimensional systems*, Advances in Physics, 51, 799 (2002); https://doi.org/10.1080/00018730110117451.
[30] M. G. Bawendi, M. L. Steigerwald, and L. E. Brus, *The quantum mechanics of larger semiconductor clusters ("Quantum dots"),* Annual Review of Physical Chemistry, 41, 477 (1990); https://doi.org/10.1146/annurev.pc.41.100190.002401.

[31] S. Husain, L. A. Alkhtaby, I. Bhat, and W. Khan, *Effect of pH variation on structural and optical properties of Zn0.95Co0.05O nanoparticles,* Journal of Luminescence, 160, 311 (2014); https://doi.org/10.1016/J.JLUMIN.2014.12.024.

[32] B. Panigrahy, M. Aslam, and D. Bahadur, *Aqueous synthesis of Mn- and Co-Doped ZnO nanorods*, The Journal of Physical Chemistry C, 114, 11758 (2010); https://doi.org/10.1021/jp102163b.

[33] F. Xu, Z. -y. Yuan, G. -h. Du, M. Halasa, and B. -l. Su, *High-yield synthesis of single-crystalline ZnO hexagonal nanoplates and accounts of their optical and photocatalytic properties*, Applied Physics A, 86, 181 (2006); https://doi.org/10.1007/s00339-006-3745-3.

[34] V. Gokulakrishnan, S. Parthiban, K. Jeganathan, and K. Ramamurthi, *Investigation on the effect of Zr doping in ZnO thin films by spray pyrolysis,* Applied Surface Science 257, 9068 (2011); https://doi.org/10.1016/j.apsusc.2011.05.102.

[35] R. Elilarassi and G. Chandrasekaran, *Influence of Co-doping on the structural, optical and magnetic properties of ZnO nanoparticles synthesized using auto-combustion method,* Journal of Materials Science Materials in Electronics, 24, 96 (2012); https://doi.org/10.1007/s10854-012-0893-4.

[36] H. Zeng, G. Duan, Y. Li, S. Yang, X. Xu, and W. Cai, *Blue luminescence of ZNO nanoparticles based on Non-Equilibrium Processes: defect origins and emission controls*, Advanced Functional Materials, 20, 561 (2010); https://doi.org/10.1002/adfm.200901884.

[37] F. L. Xian, L. H. Xu, X. X. Wang, and X. Y. Li, *Crystallographic, optical and magnetic properties of Co-doped ZnO thin films synthesized by sol gel route*, Crystal Research and Technology, 47, 423 (2012); https://doi.org/10.1002/crat.201100549.

[38] J. Ding, X. Yan, and Q. Xue, *Study on field emission and photoluminescence properties of ZnO/graphene hybrids grown on Si substrates*, Materials Chemistry and Physics, 133, 405 (2012); https://doi.org/10.1016/j.matchemphys.2012.01.051.

[39] R. H. Webb, *Electron-Spin-Resonance line shape in spherical metal particles*, Physical Review, 158, 225 (1967); https://doi.org/10.1103/PhysRev.158.225.

[40] J. P. Joshi and S. V. Bhat, *On the analysis of broad Dysonian electron paramagnetic resonance spectra*, Journal of Magnetic Resonance, 168, 284 (2004); https://doi.org/10.1016/j.jmr.2004.03.018.

[41] A. Abragam and B. Bleaney, *Electron Paramagnetic Resonance of Transition Ions* (1970).

[42] I. Stefaniuk, B. Cieniek, and I. Virt, *Magnetic properties of zinc-oxide composite doped with transition metal ions (Mn, Co, Cr)*, Current Topics in Biophysics, 33, 221 (2010); http://ctbo.home.amu.edu.pl/issue33supA/files/Abstract-v33supA_221.pdf.

[43] M. Kuzma, I. Stefaniuk, and M. Bester, *Theoretical models and EPR study of Cr based diluted magnetic semiconductors*, Journal of Physics Conference Series, 213, 012035 (2010); https://doi.org/10.1088/1742-6596/213/1/012035.

[44] F. J. Brieler, P. Grundmann, M. Fröba, L. Chen, P. J. Klar, W. Heimbrodt, H. K. Von Nidda, T. Kurz, and A. Loidl, *Comparison of the magnetic and optical properties of Wide-Gap (II,MN)VI nanostructures confined in mesoporous silica*, European Journal of Inorganic Chemistry, 2005, 3597 (2005); https://doi.org/10.1002/ejic.200500366.

[45] J. M. D. Coey, A. P. Douvalis, C. B. Fitzgerald, and M. Venkatesan, *Ferromagnetism in Fe-doped SnO2 thin films*, Applied Physics Letters, 84, 1332 (2004); https://doi.org/10.1063/1.1650041.

[46] J. M. D. Coey, M. Venkatesan, and C. B. Fitzgerald, *Donor impurity band exchange in dilute ferromagnetic oxides,* Nature Materials, 4, 173 (2005); https://doi.org/10.1038/nmat1310.

Ігор Столярчук[1], Олег Кузик[1], Іренеуш Стефанюк[2], Олеся Даньків[1],
Андрій Попович[1], Андрій Столярчук[1]

Структурні, оптичні та магнітні дослідження тонких плівок та наночастинок ZnCoO, отриманих методом імпульсної лазерної абляції

[1]Дрогобицький державний педагогічний університет імені Івана Франка, Дрогобич, Україна, i.stolyarchuk@dspu.edu.ua
[2]Жешувський університет, Жешув, Польща

Тонкі плівки та наноструктури $Zn_{1-x}Co_xO$ із вмістом кобальту до 10% були отримані методом імпульсної лазерної абляції. Проведені структурні дослідження методом Х-променевої дифракції свідчать що всі отримані зразки кристалізуються в гексагональній кристалічній структурі типу вюрциту з переважною орієнтацією вздовж площини (002). Жодних інших піків, що відповідають кластерам кобальту або оксиду кобальту, не виявлено. Атомна силова мікроскопія (АСМ) та скануюча електронна мікроскопія (СЕМ) використовувалась для характеристики отриманих зразків. Як для тонких плівок так і для наночастинок $Zn_{1-x}Co_xO$ збільшення концентрації легуючої домішки кобальту призводить до зменшення ширини забороненої зони, що зумовлено проявом s,p–d обмінних взаємодій. У довгохвильовій області спектра спостерігається додаткове поглинання, яке зумовлене d–d переходами в тетраедрично координованих іонах Co^{2+}. У спектрах фотолюмінесценції було виявлено чотири смуги випромінювання, які інтерпретуються екситонними переходами поблизу краю фундаментального поглинання, а також наявністю міжвузлового цинку, вакансій кисню та іншими домішками та дефектами не тільки в об'ємі, але й на поверхнях досліджуваних зразків. Проведені дослідження спектрів електронного парамагнітного резонансу підтвердили феромагнітне впорядкування в тонких плівках та наночастинках $Zn_{1-x}Co_xO$ за кімнатної температури. Одним з найбільш ймовірних механізмів виникнення феромагнітного впорядкування є модель зв'язаного магнітного полярона.

Ключові слова: ZnCoO, магніторозчинений напівпровідник, імпульсна лазерна абляція в рідинах PLAL, тонка плівка, наночастинка, оптичне поглинання, фотолюмінесценція, електронний парамагнітний резонанс.